Real-Time Phase and Task Estimation for Controlling a Powered Ankle Exoskeleton on Extremely Uneven Terrain

Roberto Leo Medrano, *Student Member, IEEE*, Gray Cortright Thomas, *Member, IEEE*, Connor G. Keais, *Member, IEEE*, Elliott J. Rouse, *Senior Member, IEEE* and Robert D. Gregg, *Senior Member, IEEE*

***Abstract*— Positive biomechanical outcomes have been reported with lower-limb exoskeletons in laboratory settings, but these devices have difficulty delivering appropriate assistance in synchrony with human gait as the task or rate of phase progression change in real-world environments. This paper presents a torque controller for an ankle exoskeleton that uses state estimation with a data-driven kinematic model to continuously estimate the phase, phase rate, stride length, and ramp parameters during locomotion. The controller applies torque assistance based on the estimated phase and adapts the torque profile based on the estimated task variables to match human torques observed in a multi-activity database of 10 able-bodied subjects. We demonstrate *in silico* that the controller yields phase estimates that are more accurate than state of the art, while also estimating task variables with comparable accuracy to recent machine learning approaches. The controller implemented in an ankle exoskeleton successfully adapts its assistance in response to changing phase and task variables, both during controlled treadmill trials (6 able-bodied subjects) and a real-world stress test with extremely uneven terrain.**

***Index Terms*— exoskeleton, Kalman filter, control, phase**

I. INTRODUCTION

Robotic exoskeletons may someday allow us to overcome the limits of our natural bodies. Emerging lower-limb exoskeletons are capable of providing assistive joint torques to help their wearers walk and carry loads with promising outcomes, including reduced metabolic cost [1]–[5] and muscular effort [6]–[8]. Most research to date has focused on steady-state locomotion in a controlled laboratory setting where the task and phase rate (rate of continuous progression through the gait cycle) are nearly constant. This regulated environment makes it easier to design control strategies that deliver appropriate torque assistance in synchrony with the user's gait. However, control strategies based on these assumptions perform poorly outside of the laboratory, where environments are uncertain and locomotion is highly non-steady and transitory. In order for the field to study biomechanical outcomes outside of the laboratory, new control strategies are needed that explicitly account for continuously varying task and phase.

During steady-state locomotion in controlled laboratory settings, phase progression can be reasonably predicted using time normalized by the stride period. The stride period is usually estimated as the time between subsequent ipsilateral heel strike (HS) events, which can reasonably predict the next HS event during steady locomotion. This 'timing-based' approach is quite effective and widely used for controlling exoskeletons on treadmills [9]. Typically this phase estimate parameterizes a pre-defined torque profile to deliver real-time assistance through the exoskeleton's actuator(s). Recent work has demonstrated impressive reductions in the metabolic rate of level-ground treadmill walking by optimizing this torque profile in real-time [2], [3]. While this paradigm of timing-based estimation (TBE) for torque control works well in steady-state locomotion, it is not designed for more practical conditions outside the laboratory where both the periodicity of gait and the task can change sporadically.

Recent work has addressed the problem of *non-constant* phase progression in powered prostheses and orthoses by introducing phase-based[1] controllers [10]–[18], which continuously adjust the rate of phase progression to accommodate dynamic speed changes mid-stride. In contrast to the timing-based approach, these controllers estimate the gait phase online using the exoskeleton's sensors. This phase can be estimated from shank [10] or thigh motion [11]. Alternatively, Thatte *et al.* recently introduced an Extended Kalman Filter (EKF) to estimate phase and its derivative (phase rate) without relying on any particular sinusoidal pattern in the sensors [19]. This EKF was also shown to yield more accurate phase estimates in non-steady locomotion when compared to conventional timing- and EMG-based controllers. Building on this result, we pursue further improvements in estimation using the Kalman Filter framework by incorporating other variations in task beyond speed.

To handle transitions between tasks, several groups have proposed solutions rooted in machine learning classifiers. Such classifiers can detect the human's intended task from patterns in the exoskeleton's sensor signals to apply the correct task-specific controller (*e.g.*, stair ascent vs. level-ground walking) [9], [14], [18], [20]–[25]. While this approach can identify discrete changes in task, it is less ideal for detecting continuous variations within a family of tasks or handling tasks outside the training data. Recently developed gait models have introduced task variables such as ground slope or stair height that continuously parameterize the instantaneous task [26], [27]. These variables capture more of the task's features, and can thus provide more tailored assistance to the user. Controllers based on these models have been limited to measuring the task parameter only once per stride [27]—similar to the rate of phase progression before phase-based controllers were introduced. A notable exception to this paradigm is the work of Holgate *et al.* [10], which exploited the relation in the phase plane between tibia angle and angular velocity to continuously estimate gait phase and stride length. However, this relation does not hold for non-steady-state walking, nor does it extend to other joints or task variables (*e.g.*, ground inclination). Recent work has also combined ambulation mode classification with continuous task variable estimates for ramp incline, step height, and walking speed [28], but this approach uses multiple EMG electrodes, IMUs, and goniometers that may not all be available onboard an exoskeleton.

This paper introduces an EKF-based exoskeleton controller that continuously learns both the phase state (phase and phase rate) and

This work was supported by the National Institute of Child Health & Human Development of the NIH under Award Number R01HD094772 and by the D. Dan and Betty Kahn Foundation. The content is solely the responsibility of the authors and does not necessarily represent the official views of the NIH. *Corresponding author: Robert Gregg*

R. L. Medrano and E. J. Rouse are with the Department of Mechanical Engineering and the Robotics Institute, University of Michigan, Ann Arbor, MI 48109. G. C. Thomas, C. G. Keais, and R. D. Gregg are with the Department of Electrical Engineering and Computer Science and the Robotics Institute, University of Michigan, Ann Arbor, MI 48109. Contact: {leomed,gcthomas,ckeais,ejrouse,rdgregg}@umich.edu

[1]We define 'phase-based' approaches as those where the rate of phase progression can change continuously within a stride, whereas 'timing-based' approaches have a fixed rate over the stride. Note that both would fall under the category of 'phase-based' approaches according to [9].

task state (ramp and stride length) to modulate the torque profile of an assistive ankle exoskeleton in a biomimetic fashion. The EKF can indirectly estimate the gait and task parameters in real time using onboard sensors, letting the controller adapt its output quickly and in response to a continuously-varying environment. The contributions of our work include 1) introducing a new EKF phase estimator that also estimates task parameters in continuous time, 2) validating the quality of the state vector estimates using a leave-one-out cross-validation based on previously-collected motion capture data of 10 able-bodied subjects walking on various inclines at various speeds, 3) validating the EKF estimates on an ankle exoskeleton in a controlled lab environment on an instrumented treadmill which can vary speed and inclination, and 4) validating the EKF-based controller on an ankle exoskeleton during outdoor free-walking on continuously varying surfaces (the Michigan Mars Yard and the Michigan Wavefield). These contributions to exoskeleton control enable practical, real-world usage of exoskeletons that adapt their assistance during walking at non-steady-state conditions within a continuously evolving task.

II. Modelling and Estimating Gait

A. Gait Model

Our ankle exoskeleton controller is based on a biomechanical model of gait kinematics. This model predicts global shank angle θ_s, global foot angle θ_f (see Fig. 1), forward foot position p_f, and upward foot position p_u. As input, the model takes in a gait-state vector x,

$$x(t) = \begin{pmatrix} p(t) & \dot{p}(t) & l(t) & r(t) \end{pmatrix}^T, \tag{1}$$

comprising a phase (or normalized time) signal p, its time derivative $\dot{p}$, a stride length signal l, and a ramp angle signal r. The phase variable ranges from 0 to 1 and increases monotonically throughout strides, resetting at ipsilateral heel-strikes. We denote this kinematic model,

$$\begin{pmatrix} \theta_s(t) & \theta_f(t) & p_f(t) & p_u(t) \end{pmatrix}^T = h_{\text{gait}}(x(t)). \tag{2}$$

This gait model is used to infer the gait-state vector from the measurable quantities in real-time using the framework of the Extended Kalman Filter. Using the gait-state estimate, the controller then applies the corresponding bio-mechanical torque using a second model, and this allows torque profiles to vary continuously with incline angle and stride length. We use global angles and foot positions, as opposed to joint angles, because of the convenient relationship between global foot angle and ramp inclination during stance, and because they can be either measured directly or estimated with IMUs.

1) Constrained Least-squares Regression: The model $h_{\text{gait}}(x)$ is based on labeled training data from a 10-subject able-bodied dataset [26]. This dataset contains individual stride walking data over a range of speeds (0.8, 1, and 1.2 m/s) and inclinations (-10 to 10 degree inclination in increments of 1.5 degrees). Each stride features 150 samples of kinematic and kinetic data, from which we calculated phase progression over the stride. Thus the dataset provides labeled tuples of $(\theta_s(t), \theta_f(t), p_f(t), p_u(t), x(t))$ for all (>25,000) individual strides.

We structure $h_{\text{gait}}(x)$ as

$$h_{\text{gait}}(x) = \phi^T R^T(x), \tag{3}$$

where $\phi \in \mathbf{R}^{160\times 4}$ is a matrix of real-valued model parameters and $R : \mathbf{R}^4 \mapsto \mathbf{R}^{1\times 160}$ is a gait-state-dependent regressor row-vector. The parameters ϕ are chosen to minimize the sum squared error for the equation

$$\begin{pmatrix} \theta_s(t) & \theta_f(t) & p_f(t) & p_u(t) \end{pmatrix} = R(x(t))\phi, \tag{4}$$

over all the sets of $(\theta_s(t), \theta_f(t), p_f(t), p_u(t), x(t))$ in the dataset.

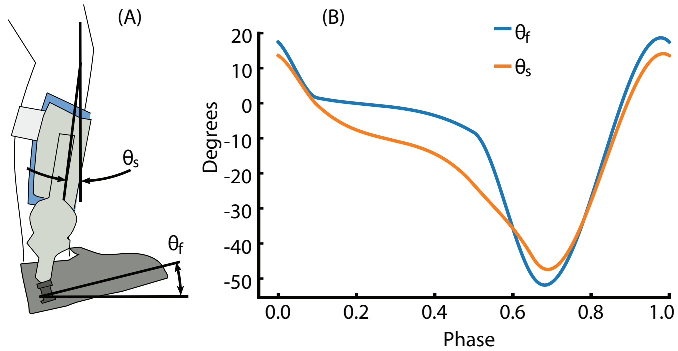

Fig. 1. (A) A sagittal-plane view of the human leg. The foot angle $\boldsymbol{\theta_f}$ is defined from the global horizontal, and the shank angle $\boldsymbol{\theta_s}$ is defined from the global vertical. (B) Average $\boldsymbol{\theta_f}$ and $\boldsymbol{\theta_s}$ profiles at zero ramp and at 1 m/s over the gait cycle.

The regressor $R(x)$ heavily uses the Kronecker product, $\otimes$, in its construction. The Kronecker product of row-vectors $A \in \mathbf{R}^{1\times N}$ and $B \in \mathbf{R}^{1\times M}$, denoted $A \otimes B \in \mathbf{R}^{1\times NM}$, is the block row-vector $(a_1 B \quad a_2 B \quad \cdots \quad a_N B)$. For matrices $A \in \mathbf{R}^{n\times N}$, $B \in \mathbf{R}^{m\times M}$, this generalizes to

$$A \otimes B = \begin{pmatrix} a_{11}B & a_{12}B & \cdots & a_{1N}B \\ a_{21}B & a_{22}B & \cdots & a_{2N}B \\ \vdots & \vdots & \ddots & \vdots \\ a_{n1}B & a_{n2}B & \cdots & a_{nN}B \end{pmatrix} \in \mathbf{R}^{nm\times NM}. \tag{5}$$

To give a relevant example, letting $\Lambda_1(x_1) = [1,\ x_1]$ and $\Lambda_2(x_2) = [1,\ x_2]$, the combined model $\Lambda_1(x_1) \otimes \Lambda(x_2) = [1, x_2, x_1, x_1 x_2]$ represents a basis for functions which depend linearly on both x_1 and x_2.

Using a series of Kronecker products, we define the regressor

$$R(x) = \Lambda_r(r) \otimes \Lambda_l(l) \otimes \Lambda_p(p), \tag{6}$$

which combines the effects of the four simpler behaviors such that the final model depends on p, l, and r. The components are:

- The ramp angle basis $\Lambda_r : \mathbf{R} \mapsto \mathbf{R}^{1\times 2}$ is a first-order polynomial Bernstein basis [29] in ramp angle,

$$\Lambda_r(r) = \begin{pmatrix} r & (1-r) \end{pmatrix}, \tag{7}$$

which allows for continuous adjustment to ground slope.

- The stride length basis $\Lambda_l : \mathbf{R} \mapsto \mathbf{R}^{1\times 2}$ is another first-order Bernstein polynomial basis in stride length,

$$\Lambda_l(l) = \begin{pmatrix} l & (1-l) \end{pmatrix}, \tag{8}$$

which similarly allows for kinematic changes associated with step length.

- Finally, the phase-polynomial basis $\Lambda_p : \mathbf{R} \mapsto \mathbf{R}^{1\times 2N}$ is a Fourier series basis of order N, defined as

$$\Lambda_p(p) = \begin{pmatrix} 1, \cos(1\cdot 2\pi p), \sin(1\cdot 2\pi p), \ldots \\ \cos(N\cdot 2\pi p), \sin(N\cdot 2\pi p) \end{pmatrix}. \tag{9}$$

where $N = 20$.

2) Least-squares Constraints: The elements of the parameter matrix ϕ are subject to constraints to produce some advantageous behavior of the resulting gait model $h_{\text{gait}}(x)$ The constraints guarantee that the $h_{\text{gait}}(x)$ function 1) predicts constant kinematics if stride length is zero (*e.g.*, if the person is stationary, the measurements do not change with respect to phase), and 2) predicts the global foot

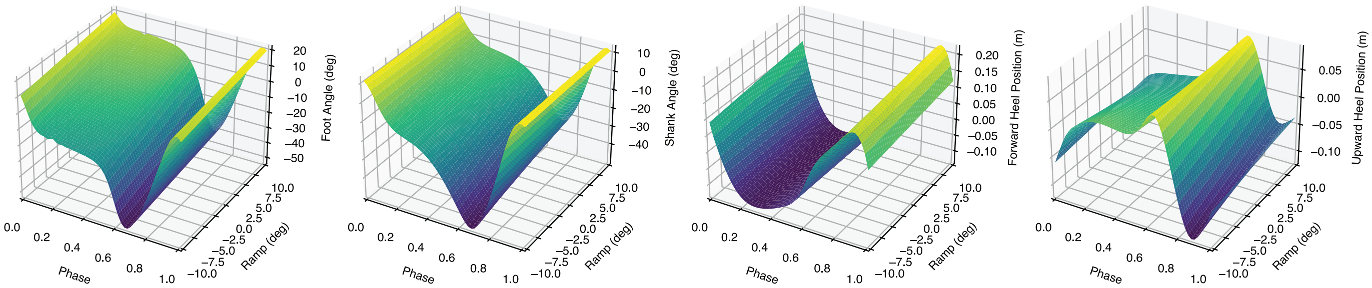

Fig. 2. The regressed continuous gait models for $\boldsymbol{\theta_f}$, $\boldsymbol{\theta_s}$, $\boldsymbol{p_f}$, and $\boldsymbol{p_u}$. As the models themselves depend on three variables ($\boldsymbol{p}$, $\boldsymbol{l}$, and $\boldsymbol{r}$) and each produce an output, they fully reside in 4D-space and are thus difficult to express in 3D-space. In this figure, the model relation between phase and ramp is shown (with stride length constant at 1 meter). Stride length merely changes the amplitudes of the gait model.

angle is equal to the ramp angle when stride length is zero or when phase takes the value 0.2.

We first define a set of two constraints to ensure constant-with-phase behavior when stride length is zero, *i.e.*, when the person is standing still. The first constraint concerns the case where both stride length l and ramp angle r are zero. In this case, we expect global foot angle θ_f, global shank angle θ_s, forward heel position p_f, and upward heel position p_u to be zero, which we express using the following matrix equality:

$$\overbrace{\Lambda_r(0)\otimes\Lambda_l(0)}^{\text{if } r=10 \text{ and } l=0,}\otimes\overbrace{\begin{pmatrix}0 & I_{2N}\end{pmatrix}}^{\forall\ p}\phi=\overbrace{0\in\mathbf{R}^{2N\times 4}}^{\text{non-constant terms are zero}}, \qquad (10)$$

which is again exploiting the behavior of the Kronecker product to achieve our aim.

To finish our pair of constraints for the case where the human is standing still, we consider the case where the ramp angle is non-zero and the stride length is zero. In this case, the shank is vertical and the foot is aligned with the ramp, while the heel positions are assumed to be at zero position. Since our model is linear in ramp angle, we only need to apply another constraint comparable to (10) to ensure this linear relationship everywhere. We choose—without loss of generality—$r = 10$ and apply the constraint

$$\overbrace{\Lambda_r(10)\otimes\Lambda_l(0)}^{\text{if } r=10 \text{ and } l=0,}\otimes\overbrace{\begin{pmatrix}\Lambda_p(0)\\ \Lambda_p(\frac{1}{4})\\ \Lambda_p(\frac{1}{2})\\ \Lambda_p(\frac{3}{4})\end{pmatrix}}^{\forall\ p}\phi=\overbrace{\begin{pmatrix}10 & 0 & 0 & 0\end{pmatrix}\otimes 1_{16\times 1}}^{\theta_f=10,\ \theta_s,p_f,p_u=0}. \qquad (11)$$

Next, we constrain the model to predict that regardless of stride length, the foot angle will be equal to r at $p = 0.2$ to represent flat-foot contact. We express this constraint on the foot using the following equality:

$$\begin{bmatrix}\overbrace{\Lambda_{\forall r}}^{\forall\ r}\otimes\overbrace{\Lambda_{\forall l}}^{\forall\ l}\otimes\overbrace{\Lambda_p(0.2)}^{\text{at } p=0.2}\end{bmatrix}\phi\ \overbrace{\begin{pmatrix}1\\0\\0\\0\end{pmatrix}}^{\text{selecting }\theta_f}=\overbrace{\begin{pmatrix}0\\0\\10\\10\end{pmatrix}}^{\theta_f=r}, \qquad (12)$$

where

$$\Lambda_{\forall r}=\begin{pmatrix}\Lambda_r(0)\\ \Lambda_r(10)\end{pmatrix}, \quad \text{and} \quad \Lambda_{\forall l}=\begin{pmatrix}\Lambda_l(0)\\ \Lambda_l(1)\end{pmatrix}, \qquad (13)$$

are matrices in $\mathbf{R}^{2\times 2}$ that expand the constraint to affect all values of ramp and stride length. The values $r = 0$, $r = 10$, $l = 0$, and $l = 1$ are again chosen without loss of generality to constrain the entirety of these linear functions.

3) Complete Gait Model: We performed the regressions for the foot and shank angle models using the constrained least-squares optimization function `lsqlin` in MATLAB. The resulting models (Fig. 2) not only described how the measured kinematics varied with phase, but also with ramp and stride length.

B. Biomimetic Exoskeleton Torque Profile

During the live trials, the exoskeleton provided torque assistance according to a profile parameterized by phase. We regressed this biomimetic torque profile using the biological ankle torques in our dataset such that the profile also continuously varied with stride length and ramp. The regression was performed using a near-identical regressor structure as in (4) with no constraints and with the biological ankle torque in lieu of the measured kinematics. This yielded a torque profile encoded with the same structure as the gait model in (3).

C. Dynamic Model and State Estimator

1) Primary Phase EKF Model: Our EKF-based controller largely uses the standard equations for an Extended Kalman Filter (see Appendix I). We define the state vector as the gait state in (2). The system process is encoded using the state transition matrix F:

$$F=\begin{bmatrix}1 & \Delta t & 0 & 0\\ 0 & 1 & 0 & 0\\ 0 & 0 & 1 & 0\\ 0 & 0 & 0 & 1\end{bmatrix} \qquad (14)$$

such that phase is updated by simple numerical integration of phase rate using the time stride Δt.

The state covariance matrix is defined as $P = 1e{-}3 \cdot I_{4\times 4}$. We define our process noise matrix Σ_Q as a diagonal matrix $\mathrm{diag}[0, \sigma_{22}^2, \sigma_{33}^2, \sigma_{44}^2]\cdot\Delta t$, where σ_{22}, σ_{33}, and σ_{44} are the standard deviations for $\dot{p}$, l, and r, respectively. Phase p has no process noise since it is defined using a noiseless integration of $\dot{p}$. The diagonal variances act as tunable parameters that modulate EKF performance; we empirically tuned the performance and found that $\sigma_{22} = 6e{-}4$, $\sigma_{33} = 9e{-}4$, and $\sigma_{44} = 6e{-}3$ yielded good performance with respect to phase tracking and response time.

2) Measurement Model: Within the update stride of the EKF, our observation function $h(x)$ extends the directly measurable variables θ_f, θ_s, p_f and p_u. To encode time-dependent measurement information, we also model the velocity of the foot $\dot{\theta}_f$ and shank $\dot{\theta}_s$. These velocities are defined using the differentiation chain rule:

$$\begin{bmatrix}\dot{\theta}_f\\ \dot{\theta}_s\end{bmatrix}=\begin{bmatrix}\frac{\partial\theta_f}{\partial t}\\ \frac{\partial\theta_s}{\partial t}\end{bmatrix}=\begin{bmatrix}\frac{\partial\theta_f}{\partial p}\\ \frac{\partial\theta_s}{\partial p}\end{bmatrix}\dot{p} \qquad (15)$$

where $\dot{p}$ is the estimate of the phase rate from the prediction stride and the partial derivatives of θ_f and θ_s are available analytically. The observation function is then $h(x) = \left[\theta_f, \dot{\theta}_f, \theta_s, \dot{\theta}_s, p_f, p_u\right]^T$, where θ_f, θ_s, p_f, and p_u, are available from the gait model $h_{\text{gait}}(x)$.

3) Nonlinear Stride Length Transformation: We choose to apply a nonlinear transformation to the stride length state. This transformation encodes the upper limit on a person's stride length. Furthermore, we model the smallest possible stride length as 0, which encodes backwards walking as having positive stride lengths and negative phase rates. In this transformation, the stride length is the output of an arctangent transformation [30], in which the 'pseudo-stride length' l_p is input. Additionally, in our gait model regression, the stride lengths were normalized by participant leg length L. As part of the non-linear transformation, we denormalize by participant leg length to obtain stride length l in meters. The nonlinear transformation is defined as:

$$l(l_p) = L(\frac{4}{\pi}\text{atan}(\frac{\pi}{4}l_p) + 2). \tag{16}$$

This allows a maximum normalized stride length of 4 leg lengths and floors it at 0. l_p is then the state estimated by the EKF and contained in state vector x. Similarly, the gait model $h_{\text{gait}}(x)$ takes as input l/L instead of l. However, for ease of communication, we refer to x as containing stride length l rather than its 'pseudo', denormalized counterpart, and the gait model as taking the stride length input directly. To account for this change in the Jacobian H in the update step of the EKF, we pre-multiply all partial derivatives with respect to l by $\frac{\partial l}{\partial l_p}$.

4) Heteroscedastic Noise Model: EKFs generally encode measurement noise in a *constant* Σ_R matrix, which typically denotes how trustworthy the sensors used are. However, this constant model is unable to selectively change the trust in the measurements during regions of the state space where those measurements are known to be informative. For example, we expect that for phase values corresponding to flat-foot contact during locomotion, the measurements of foot angle will be highly informative for the ramp angle, given the position constraint of foot contact. To improve the performance of our phase EKF controller, we implemented a *heteroscedastic* measurement noise matrix, that can continuously change the measurement noise matrix Σ_R defined as follows:

$$\Sigma_R(p) = \Sigma_{R,\text{sensor}} + \Sigma_{R,\text{xsub}}(p). \tag{17}$$

In our measurement noise model, $\Sigma_{R,\text{sensor}}$ is the conventional noise matrix that denotes how uncertain the sensors are, and $\Sigma_{R,\text{xsub}}$ represents the uncertainty present due to inter-subject gait kinematic variability (subscript xsub for cross-subject). $\Sigma_{R,\text{xsub}}$ captures the regions within the gait cycle where measurements are more informative due to lower inter-subject variability (Fig. 3). The matrix $\Sigma_{R,\text{sensor}}$ was defined as $\text{diag}[\sigma^2_{11,r}, \sigma^2_{22,r}, \sigma^2_{33,r}, \sigma^2_{44,r}, \sigma^2_{55,r}, \sigma^2_{66,r}]$, with each $\sigma_{xx,r}$ representing the standard deviation for $\theta_f, \dot{\theta}_f, \theta_s, \dot{\theta}_s, p_f, p_u$, respectively. In our implementation, these values were set to $1, 10, 7, 20, 0.01, 0.08$ respectively.

D. Heelstrike-based Estimation Backup

To protect the EKF controller against getting lost in its estimation, we introduced a backup process that was permitted to reset the estimator state in the event of sub-par phase estimation. This backup system fuses a similar approach to the conventional "Timing Based Estimation" (TBE, [31]), which detects heel strikes and records the timestamps for each heel strike event, with the EKF framework. Our backup plan is essentially a 'smaller' EKF that updates its phase rate estimates once per heel-strike, but estimates stride length and incline in real-time using the same measurements as the primary EKF.

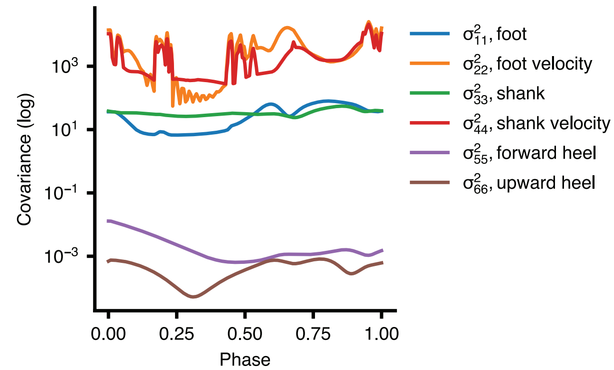

Fig. 3. The heteroscedastic measurement noise model as a function of phase. Foot angle variance $\boldsymbol{\sigma_{11}}$, foot angular velocity variance $\boldsymbol{\sigma_{22}}$, shank angle variance $\boldsymbol{\sigma_{33}}$, shank angular velocity variance $\boldsymbol{\sigma_{44}}$, forward heel position variance $\boldsymbol{\sigma_{55}}$, and upward heel position variance $\boldsymbol{\sigma_{66}}$, are shown. For ease of viewing, the covariances between these measurements are not shown.

If the backup describes a better fit to the subject's kinematics than the EKF, the backup resets the EKF state vector x with its own backup state vector. The backup system computes the sum of squares of the residuals (SSR) using the residual vector $\bar{y}$ each stride at heel-strike. It then compares its SSR to the SSR from the phase EKF (calculated using y from the EKF) over that stride. If the SSR from the backup is sufficiently smaller than the SSR from the EKF, *i.e.*, the EKF is performing poorly, then the backup overrides the EKF and places it back on course. We tuned the backup EKF to only activate once every 100 steps when the SSRs are of comparable magnitude.

III. Study Methods

Our experiments address the following hypotheses: H1) Our EKF-based controller has a significantly lower phase RMS error compared to phase estimates from a HS-to-HS timing based controller (state-of-the-art) in a leave-one-out cross validation; H2) The inclusion of incline significantly improves the phase RMS error in a leave-one-out cross validation; and H3) Our real-time EKF estimate of phase has an RMS error less than that of state-of-the-art timing based estimators in the presence of actuator torques. We also present the result of the EKF working in a practical outdoors setting with exoskeleton actuation. All human participants gave written, informed consent with approval from the University of Michigan Institutional Review Board.

A. EKF Simulation

We cross-validated our EKF *in silico* using our previously published walking dataset (N=10 subjects [26]). The trials spanned five different ramp angles between -10 and 10 degrees, and three different walking speeds (0.8, 1, and 1.2 m/s). The dataset contains walking data indexed by walking stride, which was used for training the gait model $h_{\text{gait}}(x)$. This stride data was concatenated to form a continuous walking sequence, which was then input into our EKF to see how it performed with realistic locomotion. The complete source code for our simulation is available in a ready-to-run computation capsule format through CodeOcean [32].

B. Hardware Setup

We implemented our phase EKF on an ankle exoskeleton system (ExoBoot, Dephy, Inc., Maynard, MA) for our human participant experiments. We used separate IMUs to measure each of the global angles due to the compliance of the exoskeleton's structure. We estimated the global shank angle using a custom attitude EKF [33] that ran concurrently with our phase EKF. The attitude EKF used readings from the onboard IMU (TDK Invensense MPU-9250, San Jose) mounted above the ankle joint of the exoskeleton. To measure global foot angle, we used an external IMU (3DM-CX5-25, LORD Microstrain, Williston) placed on the boot of the exoskeleton. This IMU estimated global orientation from which we obtained the global foot angle (*i.e.*, pitch angle). We calibrated both of these sensors prior to each trial to account for inter-subject differences in exoskeleton position and resting shank angle. For the angular velocity measurements, we measured the shank angular velocity directly using the exoskeleton's gyroscope readings, and measured foot angular velocity using the foot IMU's gyroscope readings. For the heel position signals, we applied a second-order linear filter to the foot IMU's accelerometer signals, which both double-integrated the forward and vertical acceleration signals to obtain forward and vertical heel positions respectively, and applied high-pass filter to these positions to compensate for integration drift.

For the indoor hardware experiment, six able-bodied, human subjects walked on an instrumented Bertec treadmill (Bertec, Columbus) with variable belt speed and inclination. The outdoor experiments were conducted with a single able-bodied human subject on both the University of Michigan Mars Yard (42.29464, -83.70898), which demonstrates an unstructured outdoor environment, and the University of Michigan Wavefield (GPS: 42.29323, -83.71168), which provides a practical stress test on extremely unsteady terrain.

C. Cross-Validation Phase Estimate Quality Experiment (H1)

To identify the ability of our EKF to adapt to new subjects while accurately estimating phase, we performed leave-one-out cross-validation on our EKF-based controller using our dataset, where ground truth phase was calculated using the normalized time between heel-strikes. For each subject, this cross-validation trained a new gait model using the individual stride data from the remaining nine subjects. We then used the concatenated stride walking data from the subject not included in the training set as the input to our EKF simulator, and computed the phase root-mean-squared-error (RMSE) of our EKF relative to the ground truth phase measurements for each stride in the dataset for that subject. To determine the improvement produced by our EKF controller, we compared the stride-wise phase errors from the EKF against the phase errors from a simulated TBE, which predicts the current phase in real-time using the normalized timings of previous heel strikes. This common method is causal whereas ground truth phase is non-causal. The TBE estimator was assumed to perfectly detect all heel-strikes from the ground truth dataset (an assumption that may not hold during practical implementations). Using a one-sided, paired t-test, we compared differences in the stride-wise phase RMSE between the EKF and TBE approaches. We also computed the stride-wise stride length and incline RMSE relative to the ground truth values from the dataset.

D. Measuring the Importance of Ramp Estimation (H2)

In a separate leave-one-out cross-validation experiment, we assess the improvement to phase estimation quality that comes from the inclusion of the ramp state in the state vector. The influence of stride length was not separately investigated because its relationship with phase estimation is more obvious due to the correlation between stride length and gait speed. To effectively eliminate the ramp state variable, elements of the process noise matrix Σ_Q and covariance matrix P corresponding to ramp were initialized to extremely low values on the order of $1e{-}12$, which prevented the estimates from changing in real time. These values were not simply set to zero in order to avoid numerical issues in the real-time computation of the state estimate. We then computed the phase RMSEs for each stride using the phase estimates of this limited EKF and determined the significance of including ramp by comparing these errors to those from the EKF using a one-sided, paired t-test.

E. Treadmill Test (H3)

We characterized our controller's performance during a controlled treadmill experiment. In this experiment, six able-bodied participants walked with the EKF-controlled exoskeleton for three segments. In the first segment, participants continuously walked on level ground for twenty seconds at 1.2 m/s, followed by twenty seconds at 0.8 m/s, followed by a return to 1.2 m/s for twenty seconds, then finally for 0.8 m/s for a final twenty seconds. In the second segment, the participants walked on the treadmill for 10 seconds at 1 m/s, then the treadmill inclined over a period of one minute and ten seconds to a maximum of 10 degrees while the participant continued walking. The third segment was identical to the second, except that instead of the treadmill inclining to 10 degrees, it declined to -10 degrees. The exoskeleton applied the adaptive biomimetic torque throughout the trials. Participants were instrumented with Vicon markers to capture their kinematics, which were then used to establish ground truth estimates for phase, phase rate, stride length, and inclination, as well as for heel-strike events. The Vicon experimental system featured 27 cameras and collected kinematic data at 100 Hz. We computed the errors and RMSEs for both EKF phase, phase rate, stride length and incline. We then compared the stride-wise phase RMSEs to those from a state-of-the-art TBE approach which thresholded the signals from the onboard device sensors to detect heel-strikes (similar to the approach from [34]); the thresholds were tuned to correctly detect heel-strikes across the walking tasks in this treadmill trial. We compared the two controllers using the same t-test as with the previous hypotheses.

F. Real-world Test

Finally, we characterized the ability of the EKF-based controller to adapt its estimates and torque assistance in a highly irregular outdoor environment. One participant from H3 walked with the EKF-controlled exoskeleton on both the Michigan Mars Yard, which features a steep hill (approximately 20 deg) covered in small rocks, and the Michigan Wavefield, which features a sinusoidal hill pattern of inclines and declines (from approximately 30° to -30°) and has been previously used to test the stability of bipedal robots [35]. These locations were chosen to 'stress-test' the EKF with non-steady-state conditions outside its training dataset. During these tests, the process noise matrix Σ_Q was tuned to have $\sigma_{22} = 1e{-}3$, $\sigma_{33} = 2e{-}3$, and $\sigma_{44} = 5e{-}2$ for a faster filter response. At the Mars Yard, the participant walked in an alternating 'slow-fast-slow' speed pattern on level ground both prior to and after ascending/descending the hill. At the Wavefield, the participant performed the same alternating speed pattern before and after walking on the rapidly changing, sinuisoidal hills. The separation of the speed and slope changes during these outdoor trials was done to isolate the EKF's ability to track each task variable independently. We recorded HD videos of these trial and compared the recorded events to the EKF's estimates to assess the adaptations to the features of the Mars Yard and Wavefield. To obtain ground truth phase values, we analyzed the video to determine the timings of heel-strike events, and interpolated phase values between them. For this experiment, we compared our EKF against a TBE identical to the one in Sec. III-D (recall TBE is causal whereas ground truth is not). We performed pairwise t-tests comparing the phase RMSE over each stride between the EKF and this TBE.

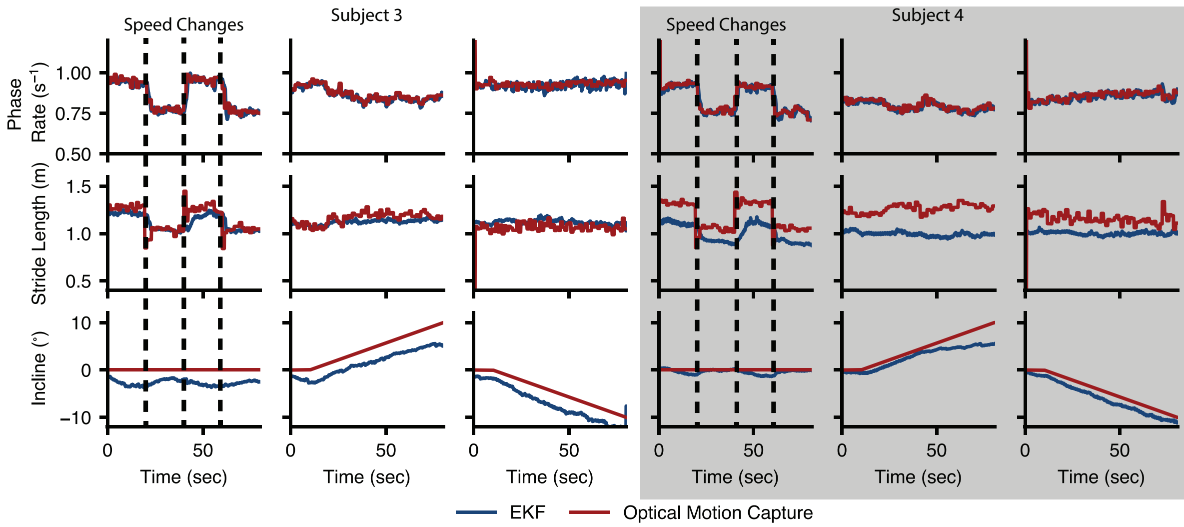

Fig. 4. State estimates from the treadmill trials from two representative participants. Phase rate is shown in the first row, stride length in the second, and incline in the third. For clarity, the periods where the speed changed in the first trial are delineated by the black dashed lines. Overall, the EKF had excellent tracking of phase rate (and thus, phase), as evidenced in these representative trials. The EKF was responsive enough to correctly estimate Subject 3's stride length but tended to underestimate this state for some participants (such as Subject 4), in part due to individual differences from the trained gait model. Finally, the EKF adequately tracked ground incline, although it occasionally exhibited a negative bias due to changes in gait caused by the exoskeleton assistance (more obvious in Subject 3).

IV. Results

A. Cross-Validation of EKF Performance

Our results support Hypothesis 1—that the EKF significantly outperforms TBE during an *in silico* leave-one-out cross validation. The inter-subject phase RMSE for the EKF ($1.6\% \pm 0.31\%$) was significantly lower ($P < 0.001$) than the inter-subject RMSE for the TBE estimator ($2.1\% \pm 0.1\%$). Additionally, our EKF predicted stride length with an inter-subject RMSE of 0.10 m$\pm$0.02 m and ramp inclination with an inter-subject RMSE of $1.5^\circ \pm 0.23^\circ$. The second cross-validation test supported Hypothesis 2—that including ramp estimation in the EKF significantly improves phase estimation when compared to an EKF that does not feature ramp estimation. The phase RMSE for the No-Ramp condition ($1.7\% \pm 0.33\%$) was significantly higher than the phase RMSE for the standard EKF condition ($P < 0.001$).

B. Treadmill Test

The treadmill test supported Hypothesis 3—that the EKF significantly outperforms TBE while applying torques. On average, the EKF (phase RMSE: $4.6\% \pm 0.84\%$) outperformed the conventional TBE approach (phase RMSE: $5.5\% \pm 0.30\%$). For five of the six subjects (Table I), the EKF significantly improved over the TBE approach ($P < 0.05$). The EKF captured the pulse-like change in phase rate during the fast 1.2 m/s and slow 0.8 m/s sections of the trials, as shown in representative trials (Fig. 4). The EKF simultaneously provided live estimates of both stride length and inclination (cross-subject average stride length RMSE 0.19 m $\pm$ 0.07 m, cross-subject average incline RMSE $2.1^\circ \pm 0.89^\circ$). The EKF clearly responded to the changes in ground inclination, although it often exhibited negative biases, as exemplified by the results from Subject 4 in Fig. 4. The EKF underestimated changes in stride length, although with notable differences in tracking quality across subjects (Fig. 4).

C. Real-world Test

In the Mars Yard trial, where the subject alternated speed and incline with exoskeleton assistance, the EKF was comparable to the conventional TBE ($3.8\% \pm 2.0\%$ for the former, $4.4\% \pm 3.1\%$ for the latter, $P = 0.2$). However, unlike the TBE, the EKF state estimates tracked both the changing speeds prior to ascending the Hill and the changing ground slope from the Hill itself. Two stills that correspond to notable events from the trial are shown in Fig. 5A and B; in particular, the position of the subject's right foot is useful to demonstrate that the EKF is updating its incline estimate correctly. On the Wavefield, the EKF significantly outperformed the conventional TBE ($4.8\% \pm 2.7\%$ for the former, $7.3\% \pm 8.3\%$ for the latter, $P = 0.02$). The extreme conditions on the Wavefield (Fig. 5C and D) rendered the steady-state assumptions of the TBE a poor fit for the gait estimation task; in contrast, the EKF was able to track both phase and the rapidly changing ground incline of the Wavefield. The EKF's adaptation of its state estimates is also reflected in the assistance from the exoskeleton. The biomimetic torque profile broadly increased the magnitude of its torque assistance when ground inclination was positive, and decreased when it was negative. This trend is reflected in the torques shown in Fig. 5. A supplemental video of the real-world experiment is available for download.

V. Discussion

As expected, our EKF phase estimator outperformed the TBE estimator, with significantly lower phase RMSEs in the *in silico* steady-state treadmill trials. Fundamentally, the EKF observes the behavior between heel-strikes, allowing it to better predict the phase variability that accompanies natural human walking, even in this steady-state test with a constant belt speed.

The presence of real-time ramp estimation within the EKF also significantly improved phase estimation. This is likely due to the ramp feature accounting for part of the variation from the kinematic sensor measurements, and therefore reducing the prediction errors. Without ramp estimation, modeling error increased, resulting in greater variance in the phase estimation signal. Hence, the task variable states could improve phase estimation during variable-incline walking compared to the phase EKF presented in [19].

In the treadmill experiment, the EKF estimator outperformed the conventional TBE in addition to providing estimates of task variables in real-time. The EKF consistently detected heel-strikes with more

TABLE I
TREADMILL TEST RESULTS

	Subject 1	Subject 2	Subject 3	Subject 4	Subject 5	Subject 6	**Average**
EKF Phase RMSE (%)	4.9	4.1	4.7	3.3	5.6	2.7	4.2 (1.1)
EKF Phase Rate RMSE (%/s)	1.5	1.8	2.4	2.7	1.9	2.0	2.1 (0.4)
Stride Length RMSE (m)	0.22	0.15	0.07	0.21	0.25	0.26	0.19 (0.07)
Incline RMSE (°)	1.0	2.7	2.8	1.2	1.8	3.1	2.1 (0.89)
Desired Torque RMSE (N-m)	2.9	3.3	2.6	2.4	3.5	3.3	2.9 (0.43)
TBE Phase RMSE (%)	5.6	5.2	5.5	4.9	5.6	3.4	5.0 (0.80)
t-test P	<0.001	<0.001	<0.001	<0.001	0.46	<0.001	N/A

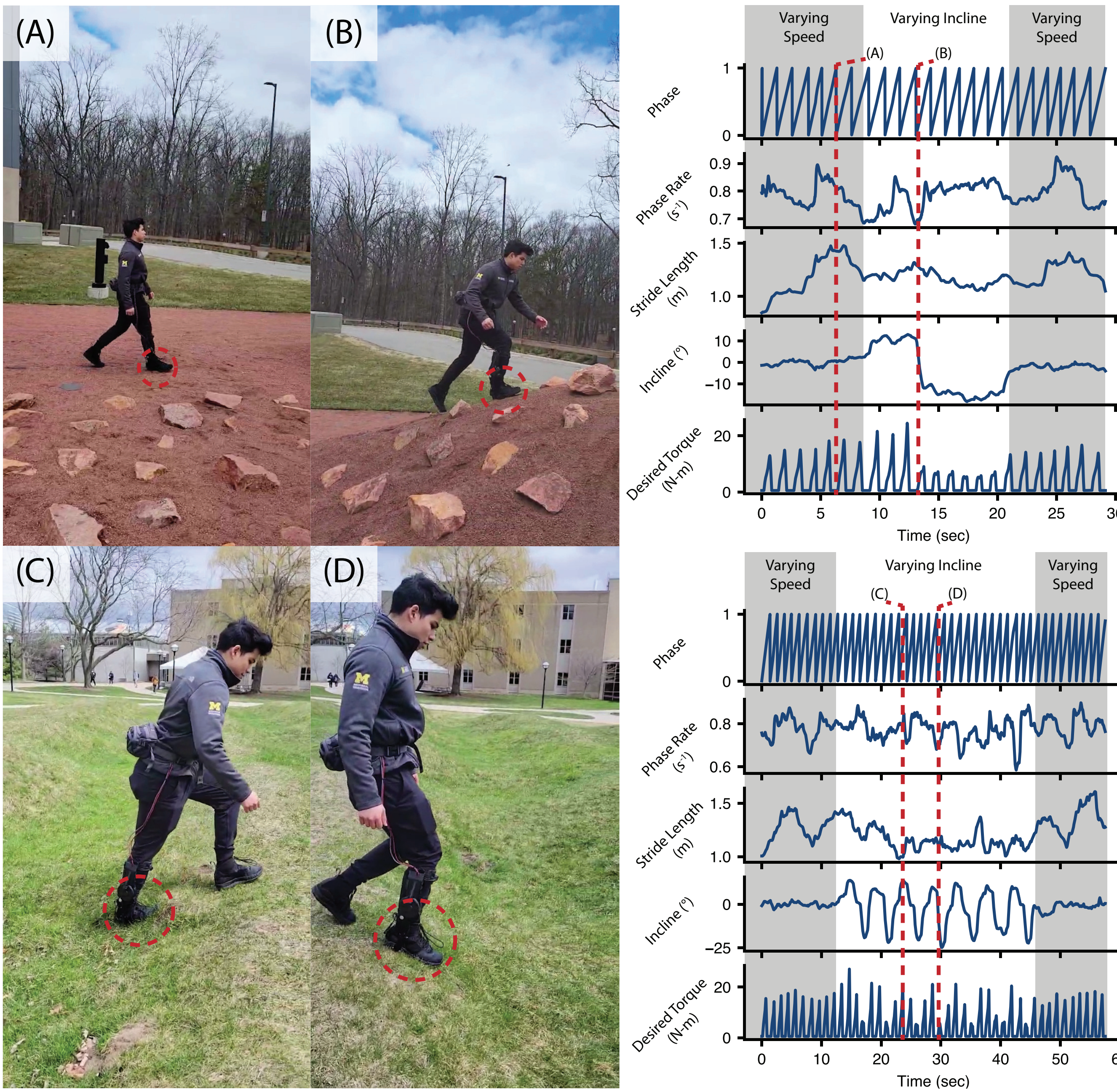

Fig. 5. Stills from the analyzed videos taken during the Mars Yard and Wavefield trials, with a focus on the EKF's incline estimation performance. The incline estimation is primarily driven by the participant's foot angle on the outdoor slopes (red dashed circles). (A) The subject walking on level ground on the Mars Yard during a period of varying speeds, with the EKF correctly updating its estimate. (B) The subject walking up the Mars Yard, in which the EKF correctly increases its incline estimate. (C) The subject walking uphill on the Wavefield (D) The subject going down a decline on the Wavefield.

accuracy than the conventional approach. Our EKF's phase RMSE (cross-subject average $4.2\% \pm 1.1\%$) is comparable to the best online phase estimation performance achieved in hip exoskeletons [14], which used machine learning to estimate phase for subjects walking through circuits that featured different ramps (phase RMSE $5.04\%^2$). Additionally, our phase RMSE is near the perceptual threshold in timing error, suggesting that subjects may be unlikely to detect any errors in torque profile assistance due to the EKF's phase error [36]. The EKF's mean incline RMSE (cross-subject average $2.1\% \pm 0.89\%$) was also comparable to recent results from an offline ML-based sensor fusion approach [28] (absolute incline error $2.3° \pm 0.86°$).

In the real-world tests, and in particular during the Wavefield stress test, the EKF estimator had a significant advantage over the conventional TBE as in the treadmill trial. The conventional TBE featured its poorest performance during the Wavefield trial (up to 7.3% from 2.1% RMSE in the steady-state cross-validation trials), due to the highly variable nature of the terrain and the non-steady-state steps taken by the participant. The EKF, in contrast, only increased to 4.2% phase RMSE during this trial.

Using an EKF confers several advantages for our adaptive torque controller. Because our simple gait model predicts angles and velocities in a fundamentally structured way, we are able to encode a large, continuous class of locomotion tasks. The EKF equations are intuitive to understand, simple to implement on hardware, and computationally lightweight, while still yielding comparable phase estimation performance to more complex machine learning approaches. Furthermore, the data-driven model component at the core of our controller may be easier to debug than so-called 'black-box' models that directly estimate gait parameters or control commands from sensor data.

Our EKF-based controller provides a solution to the challenge of estimating the state of an exoskeleton during practical trials. This challenge has been avoided in prior exoskeleton control work [1]–[4] by testing in controlled steady-state conditions that allow TBE approaches to suffice. However, these conditions are unrepresentative of the real world. The performance of our controller throughout the extreme conditions of the Wavefield test demonstrates that it can provide phase estimates throughout non-steady-state conditions, which could potentially allow exoskeleton research to be translated out of the laboratory. Additionally, our explicit gait model is agnostic to the choice of exoskeleton hardware, so our estimator could serve as a 'plug-and-play' solution for researchers seeking to take their devices into the real world.

Our EKF can also scale well to additional sensors. In our current implementation, we use four sensors (foot and shank angles, along with their derivatives, and forward and upward heel position), but it would be straight-forward to implement other sensors, such as instrumented insoles, to further improve phase estimation. We can use the current dataset to regress relationships between these sensors' measurements and our gait-state and simply extend the measurement vector in our EKF. We expect that this will further improve phase estimation due to the new information available from these sensors and motivates future study into the impact of different sensors on gait state estimation.

To further improve our estimates in future work, we would first target the inter-person variability that dominates the model fit errors [27]. Every person walks differently, and this inter-person kinematic variation increases the variance of not only the estimated phase, but also the remaining state vector elements. We suspect that inter-person variation is responsible for the large stride length RMSEs experienced by some subjects, such as Subject 6 (0.26 m RMSE, Tab. I). Stride length estimation is primarily informed by the amplitude of the forward and upward heel position measurements. When analyzing Subject 6's forward heel positions (Fig. 6A), there is a large discrepancy between the predicted position from the EKF's gait model (blue), which used the EKF's state estimates as inputs, and the predicted position from the gait model when using the ground truth states from Vicon (green). In real-time, the EKF compares the predicted positions to the actual position measurements (red) and estimates the best fit gait state that matches the measurements. For Subject 6, the stride length that produced the best-matching predictions was smaller than the ground truth stride length. This is likely because the actual position measurements provide a better fit to the smaller stride length model earlier in stance, where these measurements are thought to be more trustworthy by the measurement noise model. Subject 6 simply walks differently later in the gait cycle than our model predicts, in a way that the general gait model cannot capture with accurate state estimates. In contrast, Subject 3 (Fig. 6B) walks nearly identically to the general gait model prediction, and thus his state

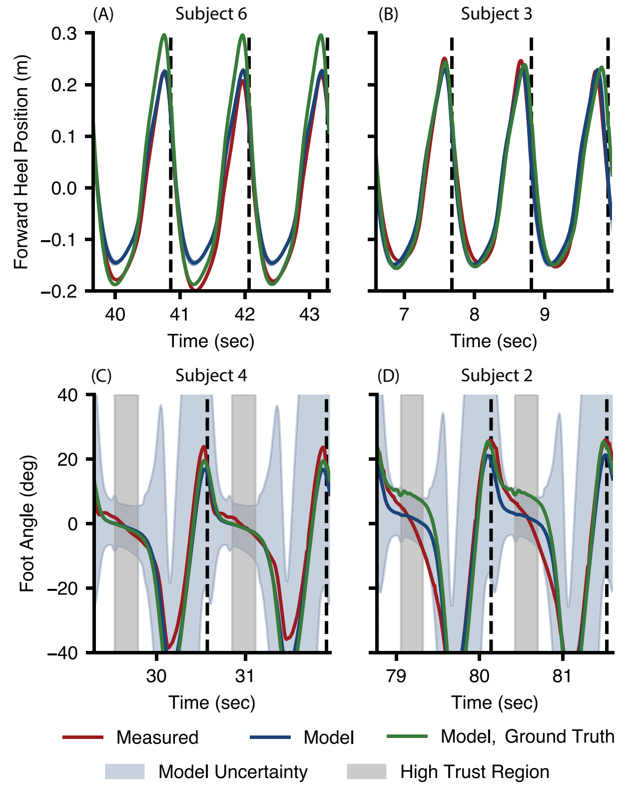

Fig. 6. (A) Subject 6's forward heel position kinematics during the treadmill trials, as an example of how inter-person gait variability can lead to errors in state estimation. Based on the subject's measured kinematics (red), the EKF gait model predicts heel positions (solid blue) that imply a state estimate which underestimates the subject's actual stride lengths; the gait model predictions using the ground truth state from Vicon (green) are a poorer fit to Subject 6's actual kinematics later in the gait cycle. (B) Subject 3's forward heel kinematics during the treadmill trials, which better match the general gait model's predictions of heel position and lead to more accurate stride length estimates. (C) Subject 4's foot angle measurements, which exhibit a clearer flat-foot contact region of the gait cycle in early stance during regions of high model trust (gray shade); trust is indicated by the width of the confidence region (blue shade) about the model estimate. and result in accurate incline estimates. (D) Subject 2's foot angle measurements, which, due to the effect of exoskeleton assistance, exhibit less-defined flat-foot contact regions where the noise model expects high confidence in the measurement, and thus result in persistent negative biases in incline estimate.

[2]Note that comparing RMSE across distinct experiments is not a direct comparison of methods.

estimates (in particular stride length) are more accurate. Simple gait personalization techniques have been shown to significantly reduce the error in gait models over a continuous range of tasks [37], so we suspect that the variance of estimated phase could be reduced with such a personalized gait model.

Unmodeled dynamics can also negatively impact our EKF performance. In particular, the exoskeleton's actuation imposes a disturbance on the system through the physical deflection of the device's IMU, which can lead to incorrect measurements of the shank angle. Our gait and heteroscedastic noise models assume that the measured shank angles will take on a specific, average profile, but actuation causes the measured shank profiles to be fundamentally different than what our models expect. In our implementation, we accounted for this by increasing the shank measurement covariance so that the EKF placed less trust in this signal. While this made the controller more robust to the disturbance caused by the exoskeleton torque, it also reduced the bandwidth of the controller, which otherwise could have been tuned to more quickly detect changes in gait.

Furthermore, the presence of exoskeleton assistance may have caused some participants to walk differently than how our gait model predicted, which would also lead to incorrect EKF behavior. For example, our gait model predicts that foot angle during early stance is relatively stationary and equal to the ground incline angle. Consequently, our noise model trusts the foot measurements during these regions of stance (Fig. 6, gray shade) as highly informative for estimating incline (Fig. 6, narrower blue bands around the predicted foot measurement during early stance). Some participants (Fig. 6C), walked similarly to this prediction while experiencing powered assistance, which led to more accurate incline estimates. However, other participants (Fig. 6D) notably had foot angle measurements that sloped downward more steeply during early stance and had a less-defined foot-contact region of stance. We suspect this is due to these participants allowing the exoskeleton's torque profile to begin lifting their foot off earlier in stance. During the region of stance where the EKF expected 1) the foot measurement to be most informative about incline, and 2) the foot angle to be equal to the ground incline, the presence of exoskeleton assistance caused the foot measurement to have a negative value relative to the ground inclination, which led to persistent incline RMSEs (which were caused due to negative errors). Here again, individualized gait models may be a potential solution, as they can capture not only how every person walks differently, but also how each person uniquely adapts their gait to exoskeleton assistance.

Because the dataset used to regress our gait model only contained steady walking data, other tasks such as running or start/stopping are not explicitly modeled. While in theory the presented EKF can account for sudden stops by estimating $\dot{p}$ as zero, we believe the estimator will benefit from training with data including such gait transitions (*e.g.*, [38]). As datasets grow to include more behaviors, our intention is to extend our continuous gait model with new task variables representing these other dimensions of human locomotion.

VI. Conclusion

We developed an exoskeleton torque controller based on an EKF which estimates phase, phase rate, stride length, and ramp in real time. This controller yields significantly reduced phase estimation errors compared to the state-of-the-art. Furthermore, this controller improves upon the state-of-the-art by allowing the assistive torque profile to adapt in real time in response to the state estimates. To the authors' knowledge, we are the first to estimate the gait phase variable along with stride length and ground inclination in real time and throughout an outdoor non-steady-state locomotion task. This result represents a meaningful milestone for practical exoskeleton control and usage outside the laboratory.

Appendix I
Extended Kalman Filter Implementation

Starting from the state estimate at the previous time $\hat{x}_{k-1|k-1}$ and the previous state covariance estimate $P_{k-1|k-1}$, our EKF implementation computes the current state estimate update using measurement z_k, dynamic model $f(\cdot)$, and measurement model $h'(\cdot)$. The process involves two steps. First, we propagate the (conveniently linear) dynamics from (14) across the time step,

$$\hat{x}_{k|k-1} = F\hat{x}_{k-1|k-1},$$
$$P_{k|k-1} = FP_{k-1|k-1}F^T + \Sigma_Q.$$

We then correct the estimate based on the measurement z_k as

$$\hat{x}_{k|k} = \hat{x}_{k|k-1} + K_k(z_k - h(\hat{x}_{k|k-1})),$$
$$P_{k|k} = P_{k|k-1} - K_k H_k P_{k|k-1},$$
$$\text{where} \quad K_k = P_{k|k-1}H_k^T\left[H_k P_{k|k-1} H_k^T + \Sigma_{R_k}(\hat{p}_{k|k-1})\right]^{-1},$$
$$\text{and} \quad H_k = \frac{\partial h'}{\partial x}|_{\hat{x}_{k|k-1}} \begin{pmatrix} 1 & 0 & 0 & 0 \\ 0 & 1 & 0 & 0 \\ 0 & 0 & \frac{dl}{dl_p} & 0 \\ 0 & 0 & 0 & 1 \end{pmatrix}.$$

Appendix II
Acknowledgements

The authors would like to thank Emma Reznick for providing invaluable training in using the Vicon motion capture system.

References

[1] L. M. Mooney, E. J. Rouse, and H. M. Herr, "Autonomous exoskeleton reduces metabolic cost of walking," *Conf Proc IEEE Eng Med Biol Soc*, vol. 11, no. 1, pp. 3065–3068, 2014.

[2] J. Zhang, P. Fiers, K. A. Witte, R. W. Jackson, K. L. Poggensee, C. G. Atkeson, and S. H. Collins, "Human-in-the-loop optimization of exoskeleton assistance during walking," *Science*, vol. 1284, no. June, pp. 1280–1284, 2017.

[3] Y. Ding, M. Kim, S. Kuindersma, and C. J. Walsh, "Human-in-the-loop optimization of hip assistance with a soft exosuit during walking," *Science Robotics*, vol. 3, no. 15, pp. 1–9, 2018.

[4] F. A. Panizzolo, G. M. Freisinger, N. Karavas, A. M. Eckert-Erdheim, C. Siviy, A. Long, R. A. Zifchock, M. E. LaFiandra, and C. J. Walsh, "Metabolic cost adaptations during training with a soft exosuit assisting the hip joint," *Scientific Reports*, vol. 9, no. 1, pp. 1–10, 2019.

[5] G. S. Sawicki, O. N. Beck, I. Kang, and A. J. Young, "The exoskeleton expansion: Improving walking and running economy," *J. NeuroEngineering and Rehabilitation*, vol. 17, no. 1, pp. 1–9, 2020.

[6] K. E. Gordon and D. P. Ferris, "Learning to walk with a robotic ankle exoskeleton," *J. biomechanics*, vol. 40, no. 12, pp. 2636–2644, 2007.

[7] T. Lenzi, M. C. Carrozza, and S. K. Agrawal, "Powered hip exoskeletons can reduce the user's hip and ankle muscle activations during walking," *IEEE Trans. Neural Systems and Rehabilitation Engineering*, vol. 21, no. 6, pp. 938–948, 2013.

[8] H. Zhu, C. Nesler, N. Divekar, V. Peddinti, and R. Gregg, "Design principles for compact, backdrivable actuation in partial-assist powered knee orthoses," *IEEE/ASME Trans. Mechatronics*, 2021.

[9] M. R. Tucker, J. Olivier, A. Pagel, H. Bleuler, M. Bouri, O. Lambercy, J. del R Millán, R. Riener, H. Vallery, and R. Gassert, "Control strategies for active lower extremity prosthetics and orthotics: a review," *J. neuroengineering and rehabilitation*, vol. 12, no. 1, 2015.

[10] M. A. Holgate, T. G. Sugar, and A. W. Böhler, "A novel control algorithm for wearable robotics using phase plane invariants," *IEEE Int. Conf. Robotics and Automation*, pp. 3845–3850, 2009.

[11] D. Quintero, D. J. Villarreal, D. J. Lambert, S. Kapp, and R. D. Gregg, "Continuous-Phase Control of a Powered Knee-Ankle Prosthesis: Amputee Experiments Across Speeds and Inclines," *IEEE Trans. Robotics*, vol. 34, no. 3, pp. 686–701, 2018.

[12] S. Rezazadeh, D. Quintero, N. Divekar, E. Reznick, L. Gray, and R. D. Gregg, "A Phase Variable Approach for Improved Rhythmic and Non-Rhythmic Control of a Powered Knee-Ankle Prosthesis," *IEEE Access*, vol. 7, pp. 109 840–109 855, 2019.

[13] I. Kang, P. Kunapuli, and A. J. Young, “Real-Time Neural Network-Based Gait Phase Estimation Using a Robotic Hip Exoskeleton,” *IEEE Trans. Medical Robotics and Bionics*, vol. 2, no. 1, pp. 28–37, 2019.

[14] I. Kang, D. Molinaro, S. Duggal, Y. Chen, P. Kunapuli, and A. Young, “Real-time gait phase estimation for robotic hip exoskeleton control during multimodal locomotion,” *IEEE Robotics and Automation Letters*, vol. 6, no. 2, pp. 3491–3497, 2021.

[15] K. Seo, Y. J. Park, J. Lee, S. Hyung, M. Lee, J. Kim, H. Choi, and Y. Shim, “RNN-based on-line continuous gait phase estimation from shank-mounted IMUs to control ankle exoskeletons,” *IEEE Int. Conf. Rehabilitation Robotics*, pp. 809–815, 2019.

[16] W. Hong, N. A. Kumar, and P. Hur, “A phase-shifting based human gait phase estimation for powered transfemoral prostheses,” *IEEE Robotics and Automation Letters*, vol. 6, no. 3, pp. 5113–5120, 2021.

[17] B. Zhang, M. Zhou, W. Xu *et al.*, “An adaptive framework of real-time continuous gait phase variable estimation for lower-limb wearable robots,” *Robotics and Autonomous Systems*, vol. 143, p. 103842, 2021.

[18] M. Shepherd, D. Molinaro, G. Sawicki, and A. Young, “Deep learning enables exoboot control to augment variable-speed walking,” *IEEE Robotics and Automation Letters*, 2022.

[19] N. Thatte, T. Shah, and H. Geyer, “Robust and adaptive lower limb prosthesis stance control via extended kalman filter-based gait phase estimation,” *IEEE Robotics and Automation Letters*, vol. 4, no. 4, pp. 3129–3136, 2019.

[20] H. Huang, F. Zhang, L. J. Hargrove, Z. Dou, D. R. Rogers, and K. B. Englehart, “Continuous locomotion-mode identification for prosthetic legs based on neuromuscular-mechanical fusion,” *IEEE Trans. Biomedical Engineering*, vol. 58, pp. 2867–2875, 2011.

[21] A. J. Young, A. M. Simon, N. P. Fey, and L. J. Hargrove, “Classifying the intent of novel users during human locomotion using powered lower limb prostheses,” *Int IEEE EMBS Conf Neural Eng*, pp. 311–314, 2013.

[22] C. D. Joshi, U. Lahiri, and N. V. Thakor, “Classification of gait phases from lower limb EMG: Application to exoskeleton orthosis,” *IEEE Point-of-Care Healthcare Technologies*, pp. 228–231, 2013.

[23] A. J. Young and L. J. Hargrove, “A classification method for user-independent intent recognition for transfemoral amputees using powered lower limb prostheses,” *IEEE Trans. Neural Syst. Rehabilitation Eng.*, vol. 24, no. 2, pp. 217–225, 2016.

[24] M. Liu, F. Zhang, and H. H. Huang, “An adaptive classification strategy for reliable locomotion mode recognition,” *Sensors*, vol. 17, no. 9, 2017.

[25] B. Hu, A. M. Simon, and L. Hargrove, “Deep generative models with data augmentation to learn robust representations of movement intention for powered leg prostheses,” *IEEE Trans. Medical Robotics and Bionics*, vol. 1, no. 4, pp. 267–278, 2019.

[26] K. R. Embry, D. J. Villarreal, R. L. Macaluso, and R. D. Gregg, “Modeling the Kinematics of Human Locomotion over Continuously Varying Speeds and Inclines,” *IEEE Trans. Neural Syst. Rehabilitation Eng.*, vol. 26, no. 12, pp. 2342–2350, 2018.

[27] K. R. Embry and R. D. Gregg, “Analysis of continuously varying kinematics for prosthetic leg control applications,” *IEEE Trans. Neural Syst. Rehabilitation Eng.*, vol. 29, pp. 262–272, 2021.

[28] J. Camargo, W. Flanagan, N. Csomay-Shanklin, B. Kanwar, and A. Young, “A Machine Learning Strategy for Locomotion Classification and Parameter Estimation Using Fusion of Wearable Sensors,” *IEEE Trans. Biomedical Engineering*, vol. 68, no. 5, pp. 1569–1578, 2021.

[29] Wikipedia contributors, “Bernstein polynomial — Wikipedia, the free encyclopedia,” https://en.wikipedia.org/w/index.php?title=Bernstein_polynomial&oldid=1033750467, 2021, [Online; accessed 31-August-2021].

[30] D. J. Villarreal, H. A. Poonawala, and R. D. Gregg, “A robust parameterization of human gait patterns across phase-shifting perturbations,” *IEEE Trans. Neural Syst. Rehabilitation Eng.*, vol. 25, no. 3, pp. 265–278, 2017.

[31] P. Malcolm, W. Derave, S. Galle, and D. De Clercq, “A Simple Exoskeleton That Assists Plantarflexion Can Reduce the Metabolic Cost of Human Walking,” *PLoS ONE*, vol. 8, no. 2, pp. 1–7, 2013.

[32] R. L. Medrano, G. C. Thomas, E. J. Rouse, and R. D. Gregg, “Extended kalman filter gait state estimation using a powered ankle exoskeleton: Adapting to changes in ramp and stride length [Source Code],” 2021. [Online]. Available: https://doi.org/10.24433/CO.1404637.v1

[33] S. J. Julier and J. K. Uhlmann, “Unscented filtering and nonlinear estimation,” *Proc. IEEE*, vol. 92, no. 3, pp. 401–422, 2004.

[34] L. M. Mooney, E. J. Rouse, and H. M. Herr, “Autonomous exoskeleton reduces metabolic cost of human walking during load carriage,” *J. NeuroEngineering and Rehabilitation*, vol. 11, no. 1, pp. 1–5, 2014.

[35] X. Da, R. Hartley, and J. W. Grizzle, “Supervised learning for stabilizing underactuated bipedal robot locomotion, with outdoor experiments on the wave field,” in *IEEE Int. Conf. Robotics and Automation*, 2017, pp. 3476–3483.

[36] X. Peng, Y. Acosta-Sojo, M. I. Wu, and L. Stirling, “Actuation timing perception of a powered ankle exoskeleton and its associated ankle angle changes during walking,” *IEEE Trans. Neural Systems and Rehabilitation Engineering*, 2022.

[37] E. Reznick, K. Embry, and R. D. Gregg, “Predicting Individualized Joint Kinematics over a Continuous Range of Slopes and Speeds,” *Proc IEEE RAS EMBS Int Conf Biomed Robot Biomechatron*, pp. 666–672, 2020.

[38] E. Reznick, K. Embry, R. Neuman, E. Bolivar-Nieto, N. P. Fey, and R. D. Gregg, “Lower-limb kinematics and kinetics during continuously varying human locomotion,” *Scientific Data*, vol. 8, no. 1, pp. 1–12, 2021. [Online]. Available: https://doi.org/10.1038/s41597-021-01057-9